SLAC-PUB-6526
June 1994
(A)

A Hybrid Anode Reactor for the SLAC Modulator *

A.R. Donaldson
Stanford Linear Accelerator Center, Stanford University, Stanford, CA 94309

Abstract

The SLAC modulators operate at 150 MW peak outputs at 120 pps with an average power of 87 kW. In an effort to improve modulator performance and reliability, we describe the design of a hybrid anode reactor using ferrite to decrease the ringing of the modulator output pulse, and incidentally reduce thyratron commutation loss. The design uses MnZn ferrite as a saturable lossy element to decrease the ringing in combination with NiZn ferrite as a saturable reactor for reducing the switching loss. The output ringing is product of the PFN stray capacitance and the leakage inductance of the pulse transformer, and if not suppressed causes premature failures of the output cable. The saturable switch aspect then offers the necessary rise time and pulse width recovery. While these two goals seem contrary, our initial performance objectives were met. Ringing on the output pulse is decreased by 50%. Switching loss reduction is measured by a thyratron temperature decrease of 15% as measured on the anode with a cathode reference temperature. The reactor packaging is very simple, and it is separated from the thyratron space so not to complicate thyratron replacement or modulator repairs and maintenance.

INTRODUCTION

The linac modulators were designed and built in the 60's, upgraded for the SLAC Linear Collider in the mid 80's, and despite their age but because of superb care, are still the backbone of a productive accelerator facility [1].

150 MW MODULATOR DATA		
Repetition Rate	120	Hz (maximum)
Thyratron Anode Voltage	46.7	kV
Thyratron Anode Current	6225	A
Pulse Transformer Ratio	1:15	
Voltage Pulse Width	5.0	μs (ESW)
Voltage Pulse Flattop	3.25	μs
Pulse Rise Time	0.8	μs
Pulse Fall Time	1.8	μs
Pulse Flattop Ripple	± 0.25	%
Nominal PFN Impedance	4	Ω
Total PFN Capacitance	0.70	μF
Charging Inductance	2.4	H
PFN Charging Time	4.1	ms
Peak Charging Current	12.7	A
5045 KLYSTRON DATA		
Klystron Frequency	2856	MHz
Klystron Beam Voltage	350	kV
Klystron Beam Current	414	A
Microperveance	2	
Peak Power Out	67	MW
Peak Input Power	500	W
Power Gain	50	dB (minimum)
RF Pulse Width	3.5	μs

TABLE I 150 MW modulator and 67 MW klystron specifications.

Table I presents the modulator specifications and sets the parameters for the design of the anode reactor. The reactor must operate at 50 kV and handle 6225 A. The unit must not reduce the pulse flat top to less than 3.25 μs which implies minimum degradation of the present rise time.

I. REDUCING THE OUTPUT RINGING

Figure 1 is a waveform showing the oscillation at the modulator output as measured on the triaxial cable in the modulator. This is the cable that exits the cabinet to connect to the pulse transformer tank. This voltage ringing is a result of the PFN stray capacitance discharging into the pulse transformer leakage inductance and a cable impedance to load mismatch ($Z_{cable} > Z_{load}$). In this circuit stray capacitance is impossible to eliminate, and while it would help, lowering the impedance of the cable is also a difficult process with only a minor effect.

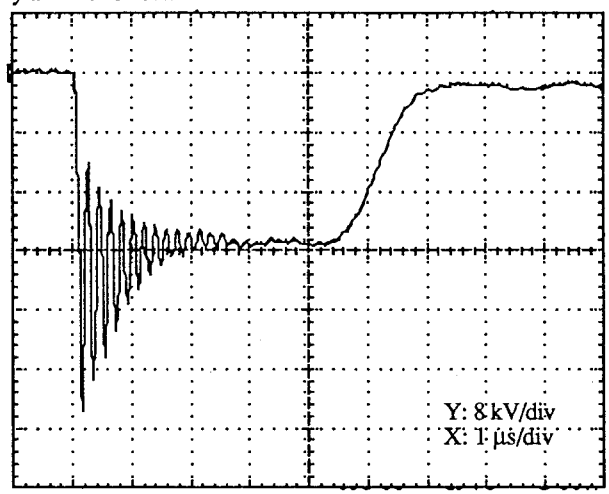

Figure 1. The output pulse and oscillation.

The oscillation can ring up to 50 kV, essentially twice the output voltage, and severely stress the dielectric in the cable. Cable lifetime (MTBF) for a 120 Hz rep rate is approximately 14,000 hours. It typically requires an hour to replace a cable, thereby reducing modulator availability [2]. Cable failures also result in damage to other modulator components. Occasionally the cable socket on the pulse transformer tank is damaged which then requires klystron and tank replacement. The goal for cable lifetime is 30,000 hours so that a cable replacement is on a par with actual klystron lifetime.

Two circuit techniques were considered for reducing the output ringing; reactive turn-on control of the thyratron, and resistor-capacitor snubbing across the cable. Realizing the requirements presented for modulator performance and availability, the reactive technique was chosen as the most practical, reliable and compact. The snubber circuit would require a resistor and capacitor, two high voltage and low inductance components, consequent high voltage terminations, and isolation from conductive surfaces in a very restricted space within the cabinet.

Another benefit of the ferrite approach would be the possibility of compensating for the slower rise time through the introduction of a saturable element in the overall circuit. The saturating ferrite could retard the thyratron current transfer and decrease commutation losses, thereby increasing thyratron lifetime [3],[4]. This latter effect is of course moderated by the initial goal of controlling the output pulse ringing.

II. SELECTING THE FERRITE

Ferrite selection for overshoot reduction is not as straight forward as selecting ferrite for a saturable switching element. The ferrite should exhibit some definite hysteresis along with high permeability, and high B_{max} swing. The hysteresis provides the lossy reactive aspect for suppressing ringing while the high μ and B_{max} allow some control of thyratron turn-on.

CMD5005 was the first ferrite tested in the modulator. This is an excellent material for fast kicker magnets and is thoroughly characterized for high frequency applications. A supply of various sized toroids were available for early testing. But realizing that the CMD5005 is often used as a saturable switch, three other materials were acquired and investigated. All are listed with their respective manufacturers and test data in Table II. A test set was used to generate B-H plots for individual ferrites. Sets of specific ferrite

Work supported by the Department of Energy contract DE-AC03-76SF00515

Presented at the 21st International Power Modulator Symposium, Costa Mesa, CA, June 28-30, 1994

toroids and combination sets were installed in a modulator for full voltage and current testing.

The ferrite test set discharges a low inductance capacitor into the ferrite that is enclosed in a coaxial package with a Pearson current transformer. The switch is an FET with a 100 V/ns discharge rate. This discharge offers a high speed approach to ferrite testing. Albeit in the modulator, the discharge rate is 1 kV/ns. The test set current, dependent on the ferrite tested, was as high as 260 A.

FERRITE	CMD5005	CMD10	MN80	3C80
Material	NiZn	NiZn	MnZn	MnZn
Shape	Toroid	Toroid	Toroid	Window
B_{max} from mfg. data [gauss]	3200	4100	5000	4600
μ_i from mfg. data	1600	550	2400	2000
H_c from mfg. data [oersteds]	0.23	0.8	0.23	0.2
Test Set DC reset current [A]	1.5	9	3	9
B scale factor [gauss/div]	490	650	650	1720
B_{max} from Test Plot [gauss]	4230	3870	5940	6900
Test Set max A-turns [A-T]	260	210	180	260
H scale factor [oersted/div]	1.4	1.8	1.8	1.6
H_{max} from Plot [oersteds]	12.9	13.8	11.8	15.6
Hc from Test Plot [oersted]	0.07	0.07	0.40	0.48
Core Area [cm^2]	10.2	7.7	7.7	2.9
Path Length [cm]	25.1	19.1	19.1	21.0
Toroid ID [cm]	2.2	3.0	3.0	
Toroid OD [cm]	10.2	9.1	9.1	
Toroid Mean Diameter [cm]	8.0	6.1	6.1	

TABLE II Ferrite specifications.

The B-H plots in Figure 2 were created with a Tektronix TDS 602 Digitizing Signal Analyzer. The discharge voltage waveform is integrated within the Analyzer, and displayed on the y-axis as B, the flux density. The discharge current drives the x-axis as H, the field strength. The flux density is a function of the ferrite cross section, there are three different areas, and this accounts for the three B scale factors in Table II. Similarly, the field strength is dependent on the mean path length of the ferrite, and thus three different H scale factors are shown in Table II.

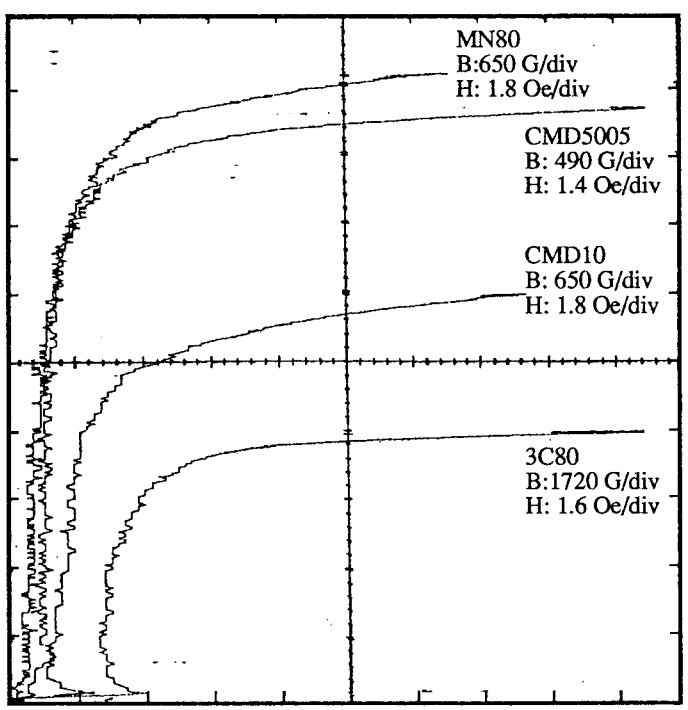

Figure 2. B-H comparisons for the ferrites. The different toroid sizes account for the various B and H scale factors.

II. Applying the Ferrite

Each of the ferrites listed in Table II requires a reset current to use the full B-H swing. In the modulator, see Figure 3, the PFN charging circuit was re-wired to provide this core bias.

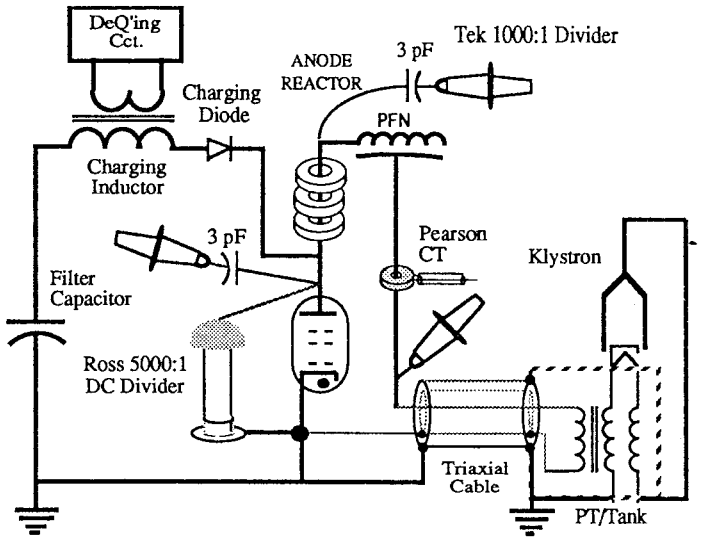

Figure 3. Simplified modulator schematic with the voltage probes and current transformer located for data collection.

The charging lead was re-routed from the first section PFN to the thyratron anode, and consequently the charging current flowing up the toroid stack in Figure 3 provides 12 A of reset.

A stack of 15 CMD5005's was tested in a modulator before the samples of the other material arrived. Figure 4 illustrates the degree of switching control that the CMD5005 stack offered. The saturation time is 130 ns, and then with the cross sectional area of the core set known, the B_{max} of the ferrite can be compared with the manufacturer and test data. The calculation gives a B_{max} swing of 3900 gauss that is within the 5% allowed for measurement error.

As expected, the 15 toroid set of CMD5005 offered a dramatic improvement in thyratron turn-on with delayed current switching, but with no reduction of the oscillation at the modulator output.

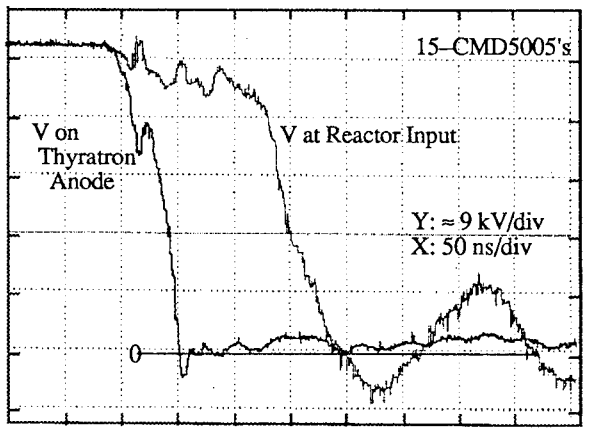

Figure 4. The delay between anode voltage fall and reactor voltage fall for the reactor set with 15-CMD5005's.

Six CMD5005's were then paired with six 3C80's. The 3C80 was used because of the price, about 1/30 the cost of CMD5005, and a significant hysteresis loop. Refer to Figure 2. This combination finally produced the intended reduction in ringing, although very modest (≈ 10%). Figure 5 shows that the voltage fall at the reactor input is no longer parallel to the thyratron anode voltage fall. This non-parallel aspect indicates that the 3C80 is introducing the hysteresis loss component. However, the fast switching CMD5005 material is over compensating for the modest loss provided by the 3C80.

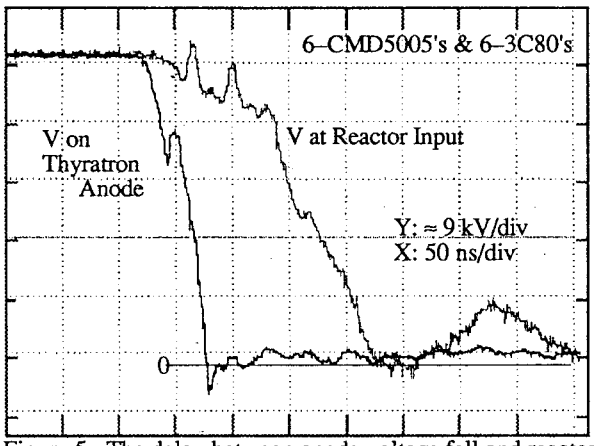

Figure 5. The delay between anode voltage fall and reactor voltage fall for the reactor set with 6-CMD5005's and 6-3C80's.

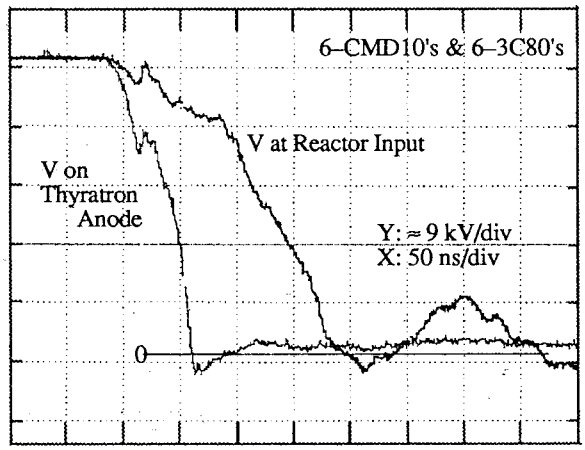

Figure 6. The delay between anode voltage fall and reactor voltage fall for the reactor set with 6-CMD10s and 6-3C80's.

The CMD10 ferrite exhibits twice the hysteresis loop of the CMD5005 with a significant increase in B_{max}, and this was the material that alone or in combination with the 3C80 resulted in major decrease in the ringing without a rise time or pulse width penalty.

Figure 6 shows the voltage fall waveforms of the CMD10 and 3C80 ferrite combination in the modulator.

Figure 7 presents output pulses for two reactor core combinations. An examination of the upper waveform in Figure 7 reveals that the peak ringing is reduced by 32 % as compared with the ringing in Figure 1 for the original modulator output.

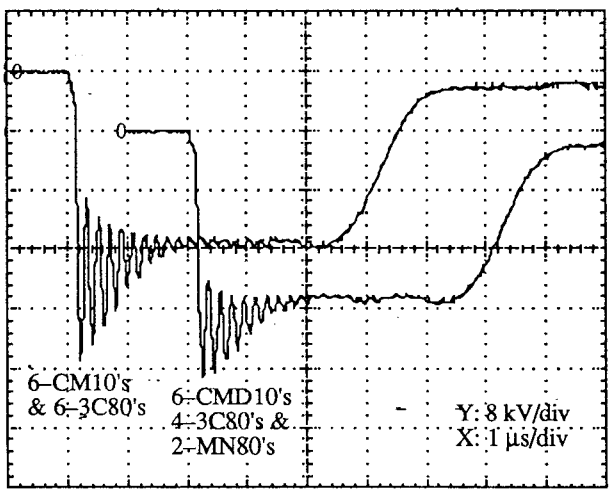

Figure 7. Comparison of output pulses for two reactor versions.

The lower waveform of Figure 7 shows the reduction in ringing for the final design. This involved replacing two of the 3C80 cores with a pair of the larger MN80 cores. In an earlier experiment, up to six additional 3C80's were added to the circuit, but as the ringing decreased, so did the pulse width at the flattop. The final reactor core combination consists of six CMD10's, four 3C80's and two MN80's. This combination resulted in a 52% reduction in peak ringing, and the 5 MHz oscillation is damped out in eight cycles as compared to the 13 cycles in Figure 1.

When the load current pulses are compared for the "no reactor" case and the two combinations above, it is as expected with the final reactor combination producing the narrowest the pulse flattop, but still within the 3.25 µs minimum that is required. With the reactor installed, the output rise time is reactor dependent, but the pulse flattop tilt and width are adjustable. The range of adjustment is a function of the excess energy in the PFN that is normally available for positive mis-match [5].

Figure 8 shows three output current waveforms with the "no reactor" and two reactor situations. There is only a minor 40 ns rise time slowdown with the CMD10, 3C80 and MN80 combination.

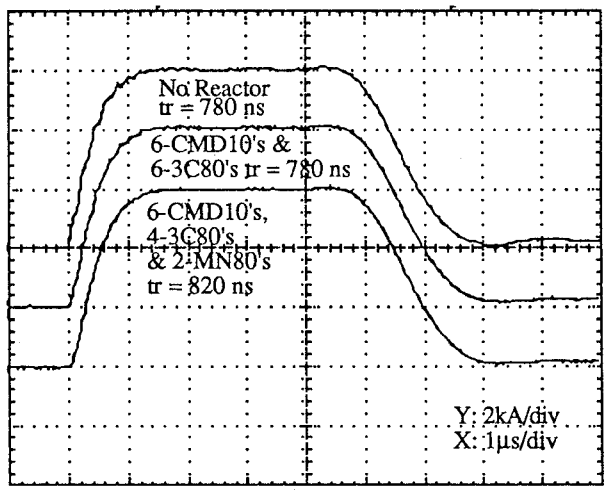

Figure 8. Comparison of output current pulses

During one phase of the design process, six MN80's were combined with six 3C80's for a 70 % reduction of output ringing, but a very narrow pulse flattop resulted that required the total PFN energy, leaving none for mis-match adjustment.

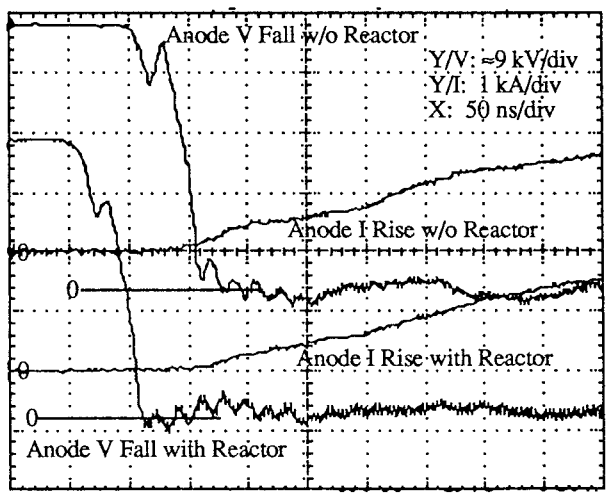

Figure 9. Comparison of time delay for anode current rise.

III. Improving Thyratron Commutation

When the voltage fall time waveforms are compared in Figures 4, 5 and 6, it is obvious that the commutation losses are increasing as more lossy ferrite is added to control the ringing. However,

Figure 6, shows that the anode fall time occurs 100 ns before the thyratron begins to conduct full current. And even when the initial current is considered as Figure 9 illustrates, the time delay between the zero anode voltage and thyratron conduction is 50 ns. The reactor must be lowering the switching loss of the thyratron.

The effect can measured and the loss difference calculated, if the discharge circuit is completely coaxial and the appropriate instrumentation exists for accurately obtaining the anode voltage fall and anode current rise [6].

Lacking the any semblance of coaxial geometry or accurate instrumentation, the anode surface temperatures were measured with and without the reactor using the thyratron deck adjacent to the cathode flange as a temperature reference and the incoming air temperature as a secondary reference.

The summary of the measurements given in Table III indicates a distinct decrease in the thyratron temperature. The mean surface temperature over the 11 sq. in. central area of the anode dropped by 3 °C. The anode hot spot temperature decreased 5 °C. This temperature reduction may increase thyratron lifetime, but it is of such modest proportions that it could take several years for the effect to be statistically noticed.

Anode Temperature Minus Reference	Surface Area sq. in.	Without Reactor °C	With Reactor °C	Temp Dec ΔT °C
T_{anode}-T_{deck}	11	20.3	17.3	3
T_{anode}-$T_{ambient}$	11	29.6	27.1	2.5
T_{anode}-T_{deck}	1	29.3	24.1	5.2
T_{anode}-$T_{ambient}$	1	38.7	34.1	4.6

TABLE III. The reactor lowers the thyratron temperature.

IV. Reactor Construction

The SLAC linac uses 244 modulators. Because of this number, any modulator improvement demands economical construction, packaging and installation. Especially considering the cost of the ferrite, even if balanced by the potential savings in cables and thyratrons.

Figure 10 illustrates the reactor assembly minus the toroid retainer. The four 3C80 are C-section ferrites that are fastened together when attached to the channel. The single reactor turn uses six parallel silicone insulated wires. The overall length of the fiberglass channel is 24 inches. The dimension determined by the width of the PFN cabinet. The toroids are spaced an inch apart to accommodate core and wire cooling.

The assembly is mounted on the PFN front panel. When the modulators were upgraded, the 20 section PFN was replaced with a 16 section circuit. The two top and bottom PFN locations were left empty. Prior to mounting the reactor, two middle PFN sections are removed and re-located to the two bottom positions. The reactor assembly then fills the space left in the middle of the PFN cabinet. The reactor is completely separated from the thyratron except for a short length a cable. This isolation permits rapid thyratron replacement without compromising repair times.

Figures 11 and 12 show the actual reactor installation in the modulator.

Figure 10. The ferrite line-up for the anode reactor.

V. Acknowledgments

The effort required to design and produce this device required several dedicated individuals. The initial effort was by R. L. Cassel, and in fact he continued as the ferrite guru until the finish of the project. T. M. Artusy provided the second installment, he generated all of the reactor voltage data and was involved in the acquisition and testing of the ferrite. C. G. Pierce, Jr. maintained the connection between the earlier work and the final installment. He made important contributions to the design, construction, installation, and testing of the reactor. The author also thanks Alfredo Saab, Department Head, Power Conversion, for his interest and encouragement.

VI. References

[1] A.R. Donaldson *et al.*, "The Second Generation SLAC Modulator," 1986 17 th Power Modulator Symposium, IEEE Conference Record CH2262-4/86/0000-230.

[2] A.R. Donaldson and J. R. Ashton, "SLAC Modulator Operation and Reliability in the SLC Era," 1986 20 th Power Modulator Symposium, IEEE Conference Record CH3180-7/92/0000-152.

[3] L. Ducimetiere and D.C. Fiander, "Commutation Losses of a Multigap High Voltage Thyratron," 1990 19 th Power Modulator Symposium, IEEE Conference Record CH2839-9/90/0000-0248.

[4] K. Rust and G. McDuff, "Life Extension of Thyratrons in Short Pulse Circuits," 1990 19 th Power Modulator Symposium, IEEE Conference Record CH2839-9/90/0000-0290.

[5] A.R. Donaldson and J. R. Ashton, *ibid.*

[6] L. Ducimetiere and D.C. Fiander, *ibid.*

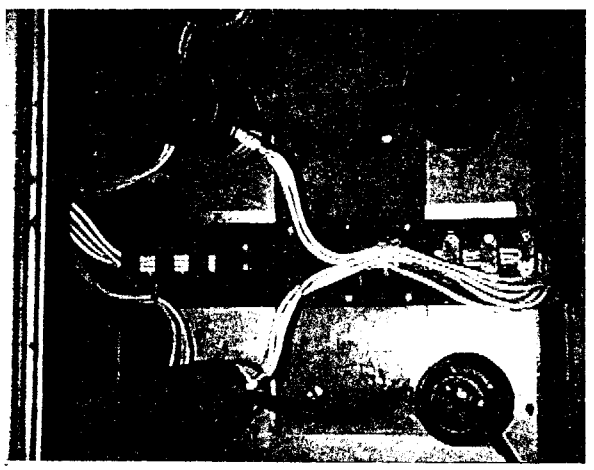

Figure 11. The reactor mounting location on the PFN cabinet.

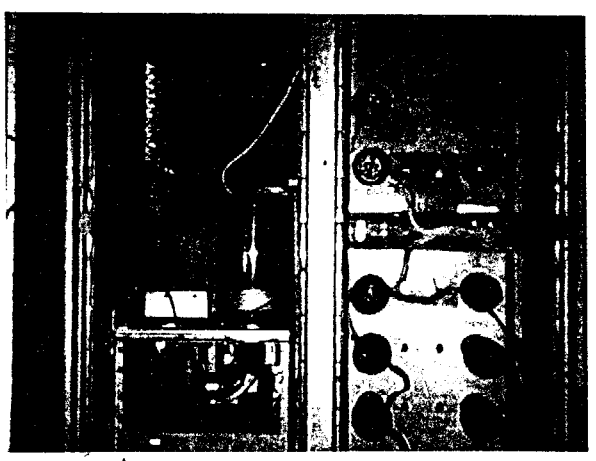

Figure 12. The thyratron, PFN and reactor in the cabinet.